# The Linkage Between Electro-Chemical Mechanical Instabilities in Battery Materials

Minal Wable $^{a,b,*}$ , Bret Marck $x^{a,*}$ , Ömer Özgür Çapraz $^b$ 

<sup>a</sup> The School of Chemical Engineering, Oklahoma State University, Stillwater, OK 74078

<sup>b</sup>Chemical, Biochemical and Environmental Engineering, The University of Maryland – Baltimore County, Baltimore, MD 21250

Corresponding Author: Ömer Özgür Çapraz; <a href="mailto:capraz@umbc.edu">capraz@umbc.edu</a>

\*Equal contribution

# **Abstract**

The battery chemistry must be diversified to achieve a sustainable energy landscape by effectively utilizing renewable energy sources. Alkali metal-ion, all-solid-state, metal-air batteries, and multivalent batteries offer unique cost, safety, raw material abundance, energy, and power density solutions. However, realizing these "Beyond Li-ion batteries" must uncover their working principles and performance & property relationship. In this aspect, mitigating chemo-mechanical instabilities in the structure and surface of the electrodes plays a crucial role in their performance. Unfortunately, the coupling between electrochemical and mechanical interactions is often poorly understood due to a lack of operando characterization. This review article explains the working principles of curvature measurement and digital image correlation for measuring stress and strain generations in battery materials. We provided specific examples of how these operando mechanical measurements shed light on instabilities in alkali-metal ion electrodes, solid electrolytes, Li-O<sub>2</sub> batteries, and aqueous Zn-ion batteries. Operando mechanical measurements offer an effective way to map changes in the physical fingerprint of the battery materials, therefore providing crucial information to elucidate instabilities in battery materials.

**Keywords:** curvature measurement, digital image correlation, solid-electrolyte interface, cathode-electrolyte interface, particle fracture, diffusion-induced stress

#### 1. INTRODUCTION

Li-ion batteries have dominated the portable energy storage landscape since their first commercialization in the early 1990s. Since then, they have powered portable electronic electrical vehicles and houses. Their successful performance has allowed to harvest renewable energies and store excessive energy as electricity using Li-ion batteries.[1] However, Li-ion batteries cannot provide the ultimate solution required to adapt renewable energy sources at a larger scale worldwide due to their limited power density and raw materials on the earth's crust. Society must consider diversifying battery chemistries for various application areas depending on the cost, weight, energy density, and lifetime of the battery.

Large-scale applications and lower-energy demand transportation (e.g., scooters and low-weight short-distance vehicles) value lower cost. Sodium-ion (Na-ion) and Potassium-ion (K-ion) batteries are promising candidates for large-scale grid energy storage in terms of availability of raw sources and cost reduction with minimum sacrifice on the performance. [2,3] Although Li, Na and K belong to the same alkali metal group with a single charge in their cation form, the reactivity and size of Na<sup>+</sup> and K<sup>+</sup> ions are intrinsically different than Li<sup>+</sup> ions. [4] Therefore, the physical and electro-chemical behavior of the electrode materials in response to Na<sup>+</sup> and K<sup>+</sup> ion intercalation is expected to be fundamentally different than Li<sup>+</sup> ion. [5,6] However, there is not much known about how electro-chemical reactions and transport of ions take place in electrode materials with different alkali metal ions.

Batteries must provide higher energy density for more energy-demanding applications, such as long-distance electrical vehicles. The incorporation of Li metal as an anode is a promising way to increase the energy density of Li-based batteries. [7] Due to the dendrite formation and flammability of the organic liquid electrolytes, solid electrolytes are proposed to be utilized in Li metal batteries. Li plating/stripping in the vicinity of the Li metal anode and solid electrolyte interface may lead to uneven deposition due to inevitable surface roughness on ceramic solid electrolytes. [8–11] Uneven plating eventually leads to dendrite formations and fracturing of the fragile ceramic electrolytes. Understanding the governing forces behind this chemo-mechanical deformation is limited by the limited access to operando measurements due to the challenging buried interface between Li metal and solid electrolyte.

Metal- $O_2$  batteries have also emerged as an energy storage device for high energy-demanding applications due to their high theoretical specific energy (e.g., 3500 Wh/kg for Li- $O_2$  batteries). [12] However, the practical performance of these batteries suffers from poor cycle life and low practical capacity due to severe interfacial instabilities, especially on the cathode side. [13–16] An Oxygen reduction reaction during discharge produces lithium peroxide as a primary reaction product. The insulating nature of the lithium peroxide poisons the cathode surface, leading to a detrimental capacity loss in the battery. Electrolyte chemistry and the nature of catalysts are widely investigated to avoid the deposition of lithium peroxide on the cathode surface. [17–19] Despite these efforts, fundamental mechanisms behind the interfacial instabilities are poorly understood.

Overall, chemo-mechanical phenomena plays a crucial role in the electro-chemical performance of these battery systems. The coupling between electro-chemical reactions and mechanical deformations dictates the electrified interfaces' reaction pathways, kinetic limitations, and instabilities. Therefore, understanding the fundamental mechanics and its coupling with physical phenomena in electrode-electrolyte interfaces and electrode structure in diverse battery environments is crucial to achieving a breakthrough with these "beyond Li-ion batteries." In this aspect, our group investigates the physical behavior of electrode materials in response to different alkali metal-ion chemistry by utilizing curvature measurement and digital image correlation techniques. In this short review article, we first summarized the working principles of curvature measurement and DIC techniques in battery application. Then, we outlined our efforts in structural and interfacial instabilities in Li-ion batteries, Na-ion batteries, K-ion batteries, all-solid-state batteries, and Li-O<sub>2</sub> batteries.

#### 2. OPERANDO MECHANICAL MEASUREMENTS

Curvature measurement and digital image correlation are non-destructive, non-contact, and optical techniques for probing mechanical deformations in materials.

**2.1 Curvature Measurement:** Curvature measurement techniques have been employed to monitor stress generation within the electrode materials as well as an electrode-electrolyte interface in various electrochemical systems such as anodizing[20], corrosion[21,22], electrodeposition[23–26], battery materials[27–31], electrocatalysis[32–35], electrosorption[36–38], and fuel cells[39,40]. A material of interest is typically deposited as a thin film on one side of the substrate. The substrate must be inert in applied experimental conditions, and the back side of the substrate must be reflective. The principle of the curvature measurements is based on the detection of curvature formed on the inert substrate because of the (electro)-chemical reaction induced stress in the thin film constrained by the substrate. The measured curvature of the substrate, then, can be converted into the stress-thickness product in the thin film via Stoney's equation[41–43];

$$F = \int_0^{h_f} \sigma(z) dz = \frac{E_s h_s^2 \kappa}{6(1 - \nu)}$$

where  $h_f$  is the thickness of the film, F is the in-plane force per unit width in the thin film,  $E_S$  is Young's modulus of the substrate,  $h_S$  is the substrate thickness, v is the Poisson's ratio, and the substrate curvature is denoted by  $\kappa$ .

Figure 1A-B demonstrates the principles of the curvature measurement system. A single-beam laser reflectometry technique probes the position of the single beam reflected from the back side of the

cantilever [44-46]. The technique is prone to noise and reduced stability since detection depends on the single beam position on the cantilever. Several techniques have been developed to overcome this limitation, such as scanning laser reflectometry, multi-beam optical stress sensor (MOSS), and curvature interferometry. Scanning laser reflectometry also utilizes a single beam, but it continuously monitors the backside of the cantilever, therefore reducing the noise in the measurements. [47-49] The MOSS technique, developed by Chason and Floro, probes the inplane substrate curvature by monitoring the deflection of an array of equally spaced laser beams reflected from the cantilever.[50] Phase-shifting curvature interferometry monitors the interference of the beams, which

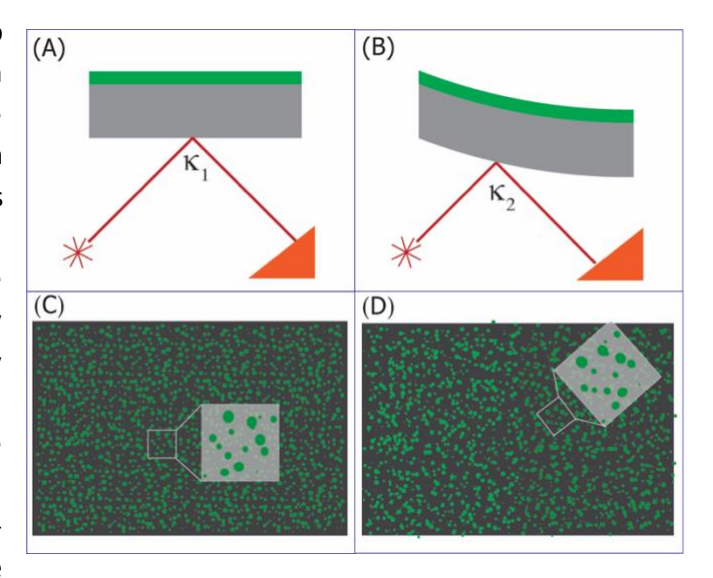


**Figure 1:** Principles of curvature measurement (A, B) and digital image correlation (C,D) techniques. (A, C) shows the undeformed electrode whereas (B,D) exhibits deformed electrodes.

can be converted into time-dependent path length difference and associated curvature in the cantilever. [20] Introducing the phase shifting in the reflected beams provides increased sensitivity and stability in the curvature measurement. Details of the MOSS and phase-shifting curvature interferometry techniques can be found in our previous publications. [20,51]

**2.2. Digital Image Correlation:** Digital image correlation (DIC) probes a full-field deformation at microstructural length scales. [52] The technique has been widely used in mechanical and civil engineering applications. Yue Qi and Stephen Harris are pioneer scientists applying the DIC to probe 2-D deformation and strain fields in Li-ion graphite electrodes. [53] Later, Shearing et al. mapped out the 3-D deformations in lithium manganese oxide via 3D X-ray computed tomography and digital volume correlation. [54] Jones et al. successfully utilized digital image correlation as an operando technique by synchronizing the electrochemical responses with the strain generation on graphite electrodes in Li-ion batteries. [55–57] Later, Koohbor et al. developed a unique cell design to adapt DIC to monitor interfacial strains in solid electrolyte—electrode interfaces. [58,59]

DIC measures deformation by tracking the changes in the speckle patterns in small neighborhoods called subsets during deformation (Figure 1C & D). Therefore, speckle patterns should be small enough to facilitate full-field measurements with high spatial resolution. The speckle patterns should also provide enough contrast with the target material. Digital image correlation requires well-defined speckle patterns to track the motion of the electrode during charging/discharging. Another requirement is ensuring good electrical connection while providing unconstrained and free-standing geometry for the battery materials. To overcome this challenge, Jones et al. and Koohbor et al. designed an electro-chemical custom cell that can mimic the performance of commercial batteries for in situ strain measurements. [55,59]

#### 3. PROBING INSTABILITIES IN BATTERY MATERIALS

#### 3.1. Structural Instabilities

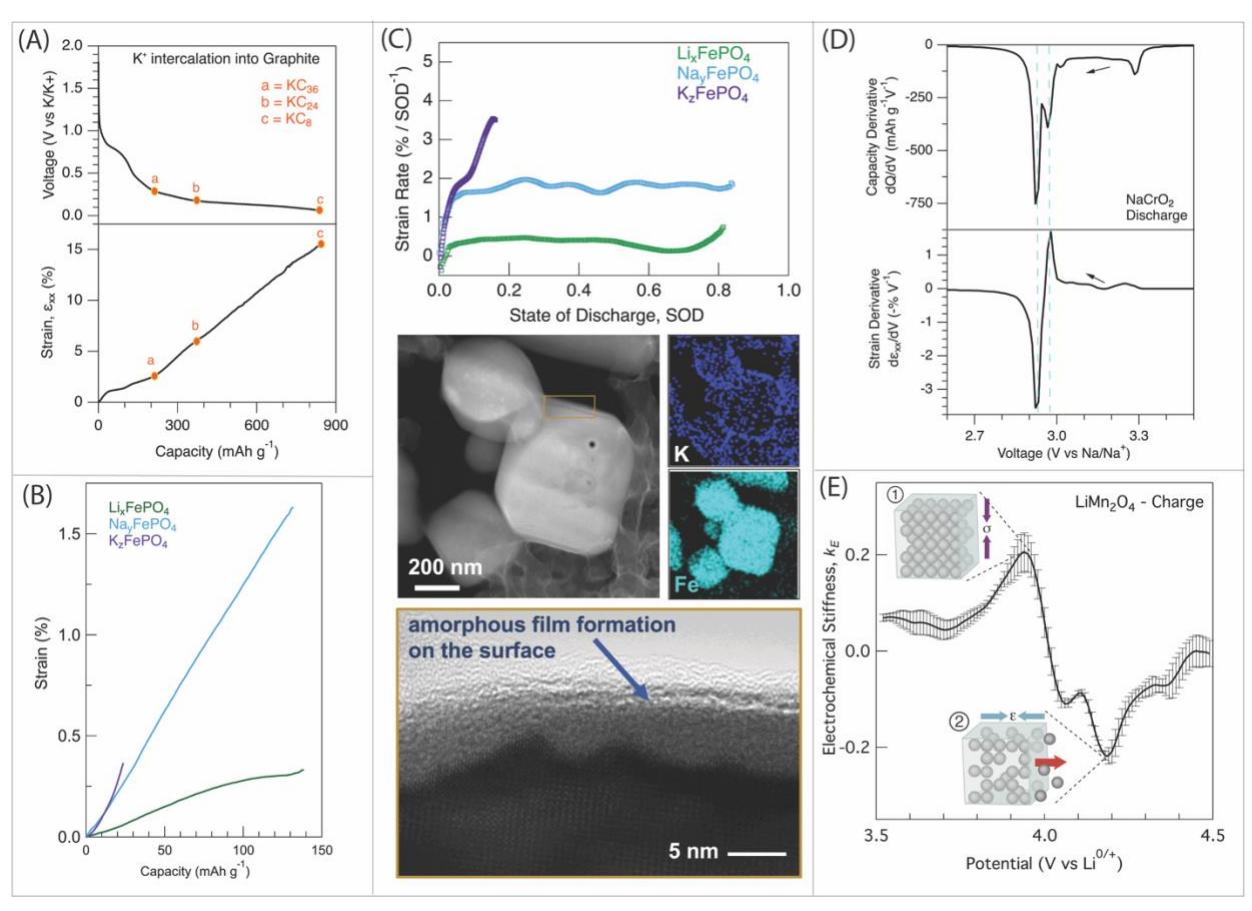


Figure 2: Mechanical deformations in battery electrodes during alkali metal ion intercalation. (A) electrochemical strains in graphite anode during K-ion intercalation (Modified with permission from ref 66); (B) Generation of electrochemical strains in iron phosphate cathodes upon intercalation of Li, Na or K ions (Modified from 67 under the terms of the Creative Commons CC BY 4.0 license); (C) Strain rate in iron phosphate cathodes upon intercalation of Li, Na or K ions and transmission electron microscopy images after K-ion intercalation into iron phosphate cathode (Modified with permission from ref 74); (D) Capacity and strain derivatives in NaCrO<sub>2</sub> cathode during Na ion intercalation; (E) Electrochemical stiffness calculation in LiMn<sub>2</sub>O<sub>4</sub> cathode by synchronizing stress and strain generation during charge (Modified with permission from ref 76).

A typical mechanism of alkali metal-ion intercalation into electrodes involves several steps, including ion transport in the electrolyte, solvation/desolation mechanisms, intercalation of ions into electrodes, phase transformation in the electrode structure, and solid diffusion of alkali metal ions. [60] Intercalation of alkali metal into electrodes leads to volumetric changes in the electrode structure and associated stress generation. Electrode's ability to accommodate the electro-chemical strains impacts the structural stabilities. Expansions in the electrode strongly depend on the crystallographic structure of the host electrode, the size of alkali metal ions, and their chemical interaction. [61]

Digital image correlation has been utilized to measure electro-chemical strains in battery electrodes during cycling. Intercalation of Li ions into composite graphite electrodes generates almost 1.5 % strain generation [57]. When K ions are inserted into graphite, the electrode experiences lead to 17.6% strain generation (Figure 2A). [62] Cathode electrodes are mostly brittle materials, and they cause severe structural instabilities even at smaller strains. [63–65]

Our team has investigated the electro-chemical strain generation in various cathode structures such as transition metal oxides, olivine-type polyanions, and Prussian blue analogs for Li, Na, and K-ion batteries. [62,66–73] Overall, there is a linear correlation between electro-chemical strains and capacity in the electrode with an expectation in iron phosphate cathode in K-ion chemistry (Figure 2B). A nonlinear correlation between strains and capacity was observed when K ions were intercalated into crystalline iron phosphate cathodes. To shed light on this discrepancy, strain rates per state-of-discharge were calculated during Li, Na, and K ion intercalation into iron phosphate cathodes (Figure 2C). [67] K-ion intercalation leads to an increase in the strain rate with the state of discharge. In situ X-ray diffraction demonstrated amorphization in the crystalline iron phosphate during K-ion intercalation, and it was verified by ex-situ high-resolution transmission electron microscopy (Figure 2C). [74] Li and Na ion insertion into iron phosphate results in nearly constant strain rates except for the first discharge with Na ions. Interestingly, Yet-Min Chiang and his group also detected anomalies only during the first discharge of Na ions into iron phosphate cathodes via in situ x-ray differentiation. [61] Overall, the operando DIC study suggests that strain rate, rather than nominal strains, is responsible for the amorphization in the crystalline electrodes. Furthermore, DIC measurements were able to capture deformations quantitively during amorphization, which opens the door to investigate chemo-mechanical instabilities in amorphous electrodes as well.

The DIC technique also provides localized changes in the electrode structure during intercalation. Despite being a microscale technique, the DIC was able to track nanoscale changes in the electrode structure associated with the phase changes. [62,66–73] Strain derivatives were calculated by taking the derivative of strain to the electro-chemical potential. The location of the strain derivatives matches very well with the current peaks in cyclic voltammetry and peaks of capacity derivatives in galvanostatic cycling. Our team recently investigated the phase-transformation-induced structural changes in transition metal oxide cathodes for Na-ion batteries. Figure 2D shows capacity (dQ/dV) and strain derivatives ( $d\epsilon/dV$ ) during the discharge of Sodium Chromium Oxide ( $d\epsilon/dV$ ) cathode in Na-ion batteries. Two strain derivative peaks around 3.0 and 2.9V align well with the capacity derivatives. Two strain derivative peaks with opposite directions indicate the distinct difference in the structural distribution in the cathode during Na insertion. The directional differences in strain derivatives result from phase transformations from P3 to O'3+P3 and O'3+P3 to O3+O'3 in the NaCrO2 structure. [75]

Synchronizing digital image correlation and curvature measurement techniques further offers opportunities to differentiate complex structural instability problems in battery electrodes. Dr. Elizabeth Jones et al. calculated electro-chemical stiffness evolution in graphite anode during discharge in Li-ion batteries by combining stress and strain measurements. [56] Electrochemical stiffness demonstrated a significant stress build-up on the electrode before Li intercalation, followed by strain-dominated deformations associated with Li insertion into graphite sheets. Later, we calculated electro-chemical

stiffness evolution in lithium manganese oxide cathodes for Li-ion batteries (Figure 2E). [76] The electrode experienced significant stress build-up before the extraction of Li from the electrode during charge, followed by strain-dominated deformation at higher voltages as the electrode underwent phase transformations. Dr. Kimberly Bassett et al. carefully analyzed the impact of electrolyte chemistry on the surface stress build-up on the model lithium iron phosphate cathode. The model electrode undergoes only one phase change, which allows deconvoluting structural instabilities with surface stress generation on the electrodes. [77] Surface stress was associated with the higher impedance in LiPF<sub>6</sub> vs. LiClO<sub>4</sub>-containing electrolytes. Based on these results, our team has been working on identifying governing forces behind the instabilities in metal oxide cathodes at higher voltages by synchronizing stress and strain measurements.

# 3.2. Interfacial Instabilities

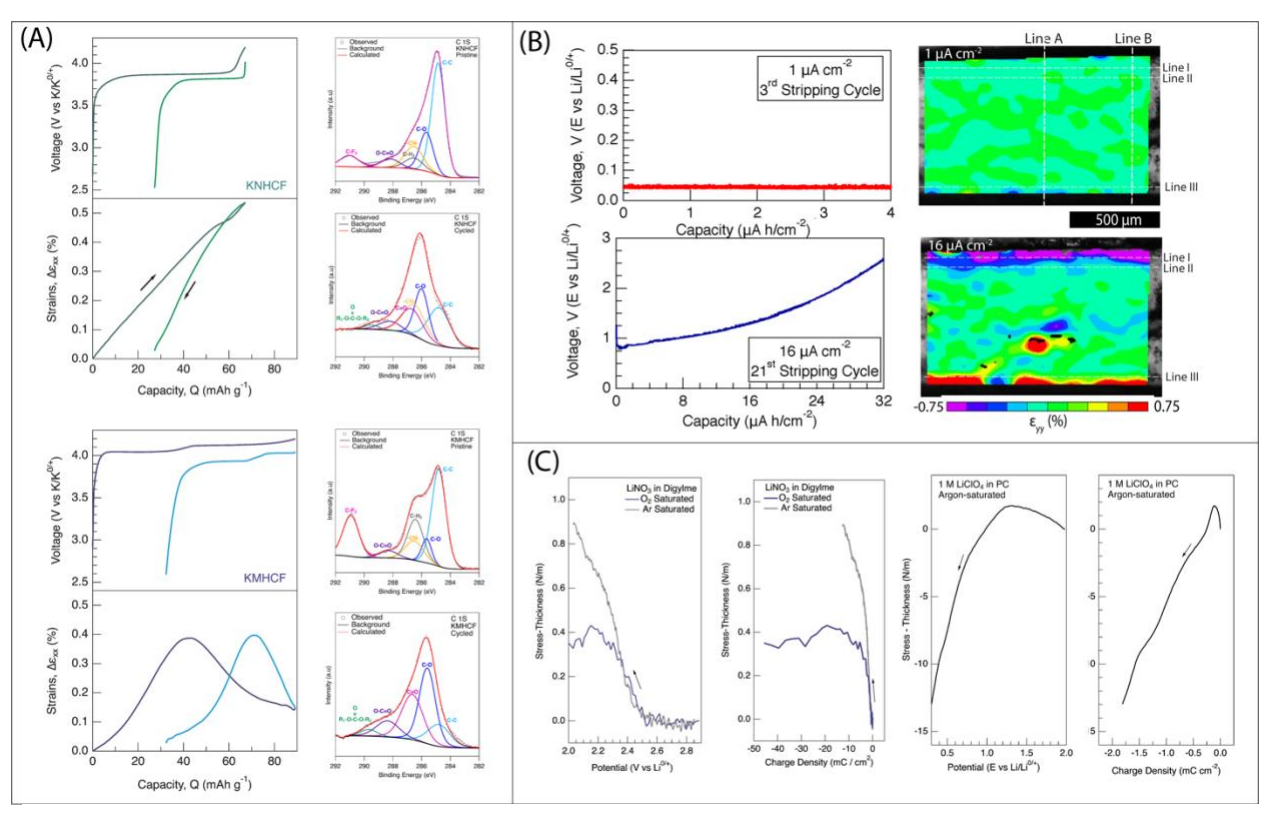


Figure 3: Interfacial deformations in electrified electrode – electrolyte interface in battery applications. (A) electrochemical strains in Ni- (KNHCF) and Mn- (KMHCF) based Prussian blue analogues cycled in 1 M KPF<sub>6</sub> in EC:PC electrolyte and associated surface chemistry analysis after cycling (Modified with permission from ref 62), (B) Generation of electrochemical strains in the LAGP solid electrolyte – Li anode during stripping (Modified with permission from ref 96) and (C) Stress-thickness product on Au positive electrode during the electrochemical polarization in either oxygen-saturated diglyme electrolyte, argon saturated diglyme electrolyte or argon-saturated PC electrolyte (Modified from ref 51 under the terms of the Creative Commons CC BY-NC-ND 4.0 license).

**3.2.1 Liquid Electrolyte – Solid Electrode Interface:** Interfacial instabilities are associated with liquid organic electrolytes' stability, compatibility, and reactivity in alkali metal-ion chemistries. The chemical

composition of the surface layers on the electrode depends on the organic solvent and type of salt in the electrolyte [78,79]. The chemistry of surface layers and the electrochemical stability of various salts and solvents have been systematically investigated for alkali-metal ion batteries. [80–87] The transport of ions across the solid-electrolyte interface (SEI) or cathode-electrolyte interface (CEI) layers and the stability of the battery components are the key factors controlling battery performance. These surface layers function as an electronic insulator, preventing the continuous consumption of the electrolyte solvents and salts. The formation of SEI / CEI layers strains the electrode's surface, causing surface stress. SEI/CEI layers influence the electro-chemical performance of the electrodes as well as the mechanical stability of the electrodes. The decomposition of organic electrolytes on the electrode surface introduces an additional barrier for ions to be inserted into or removed from the electrode structure. However, it is very challenging to identify the potential-dependent CEI layer and associated mechanical deformations because the intercalation of alkali-metal ions into the electrode structure also induces volumetric changes simultaneously.

In order to deconvolute these competing mechanisms, our team recently utilized electro-chemical characterization, X-ray photoelectron spectroscopy (XPS), and digital image correlation on Prussian blue analogs (PBA). [62] When cycled under the same conditions, Mn-based PBA suffers rapid capacity loss compared to the Ni-based PBA cathodes. DIC analysis demonstrated similar reversible electro-chemical strains during each cycle in Ni-based and Mn-based PBA cathodes (Figure 3A). This observation is quite surprising given that Ni-based PBA is often described as a "zero-strain" electrode in the literature. [88–90] XPS analyses revealed a higher presence of complex organic substances within the cathode electrolyte interface (CEI) layer developed on Mn-based PBA cathodes when contrasted with Ni-based PBA cathodes. The accelerated decline in capacity observed in Mn-based PBA cathodes, compared to nickel (Ni)-based counterparts, is linked to the augmentation of organic compounds within CEI layers rather than physical distortions.

**3.2.2 Solid Electrolyte – Solid Electrode Interface:** Investigation of fundamental interfacial instability mechanisms in solid electrolytes is challenging due to the complex nature of the solid electrolyte-electrode interface and the difficult differentiation of deformed products. [91–95] Although ex-situ techniques indicate the dramatic changes that happened on the surface and bulk of the electrolyte because of the electrochemical processes, these techniques cannot monitor what happens on the solid electrolyte surface and bulk structure during battery operations. Operando studies of the interfacial degradation process of all-solid-state batteries are crucial to formulating solid electrolyte design strategies for mitigating these degradation processes and improving battery performance.

Our team developed an operando digital image correlation method to address this need to probe deformations in the LAGP – Li metal interface during plating/stripping. [96] Figure 3B demonstrates the voltage evolution and associated counterplots for strain generation in the LAGP solid electrolyte and the Li metal – LAGP interface. DIC detected increased heterogeneity by increasing the cycle number and applied current density. Measurements indicate the correlation between the overpotential and the increase in strains in the interface. Abnormal strain generation was detected in the center of the solid electrolyte, where large fractures were detected via ex-situ Micro CT. Overall, operando DIC allowed us to monitor strains with spatial and temporal resolution and synchronize the strains with the electro-

chemical response during Li plating/stripping. We foresee that this feature will enable us to investigate how the structure & chemistry properties of solid electrolytes impact instabilities in Li anode—solid electrolyte and solid electrolyte—cathode interfaces.

**3.1.3 Triphase Interface:** The practical performance of Li-O<sub>2</sub> batteries is hindered by inadequate cycle durability and limited usable capacity attributed to unstable interfaces at the electrode surfaces. Many studies compare the chemistry of electrolytes and catalysts with the overall discharge reaction products in Li-O<sub>2</sub> batteries.

The electro-chemical reaction environment in Li- $O_2$  batteries resembles electrocatalysis, where gas phase material is electrochemically oxidized/reduced on a solid catalyst in a liquid electrolyte. [32–35] Furthermore, if the discharge reaction products favor surface-based mechanisms, one should also expect stress to be generated due to nucleation and growth of lithium superoxide and peroxide. In this manner, the surface-based mechanisms may demonstrate similarities with electrodeposition and anodizing studies. [24,97–100] Unfortunately, the role of surface stress on the electrocatalytic reaction pathways has not received any attention yet.

To fill this gap, our group developed a specialized battery cell to probe stress generation on Au electrocatalyst via a multi-beam optical sensor (MOS). The  $\text{Li-O}_2$  battery underwent discharge within a LiNO3-diglyme electrolyte using two methods: linear sweep voltammetry and constant current application, both conducted in an  $\text{O}_2$  environment. Parallel control tests in Argon-saturated electrolytes demonstrated surface stress origination from charge-induced stress (Figure 3C). The generation of stress on the positive Au electrode is ascribed to the creation of  $\text{Li}_2\text{O}_2$  reaction products on the Au surface and the stress induced by the electrocapillary. Surprisingly, the average stress-charge coefficient during oxygen reduction reaction in oxygen-saturated electrolytes was almost 2-orders smaller than the stress-charge coefficient recorded for Li-Au formation.

We want to note that instabilities in lithium superoxide reaction intermediate and lithium peroxide discharge products may originate from complex chemo-mechanical interactions. These may involve the adsorption of solvated ions and /or reaction intermediates, the chemical properties under applied electrical field variation, and changes in the surface potential during nucleation, growth, and grain formation.

# 3.3. Rate-Dependent Mechanical Deformations in Battery Electrodes

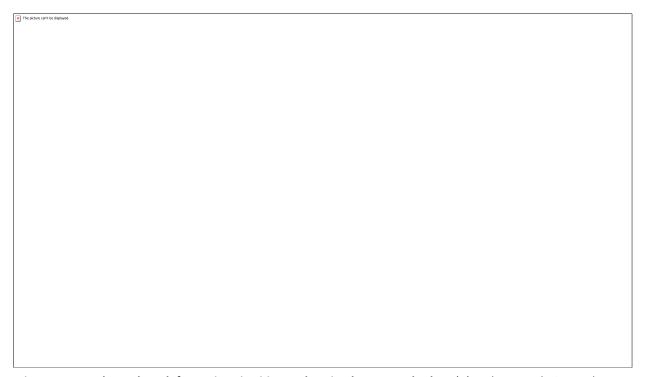


Figure 4: Rate-dependent deformations in Li-ion and Na-ion battery cathodes. (A) Voltage evolution and strain generation in NaFePO<sub>4</sub> cathode cycles at different C-rates. Dotted points indicate the predict strains calculated via mathematical model (Modified with permission from ref [72]), (B) Voltage evolution and strain generation in LiFePO<sub>4</sub> cathode cycles at different C-rates (Modified with permission from ref [71]), (C) Potential and strain evolution in LiFePO<sub>4</sub> during pulsed current charge/discharge at C/4 rate (Modified with permission from ref [71]), (D) Strain generation in LiMn<sub>2</sub>O<sub>4</sub> cathode with/out Au-coating at different C-rates. Square points indicate the predict strains calculated via mathematical model (Modified with permission from ref [73]).

The fast-charging ability of batteries is a desirable feature for many demanding applications, including electric vehicles. However, the electrodes further suffer from severe chemo-mechanical instabilities at faster charging rates, which is associated with the diffusion limitations in the electrode and the shift in the phase transformations at faster rates. The steep concentration gradients of charge carrier metal ions can develop in the electrode. These concentration gradients cause highly non-uniform volume changes and phase transformation between the electrode's surface and center. Therefore, they cause misfit strains and associated stress development in the electrode. [27,101,102] Misfit strains and concomitant stress influence the thermodynamics of electrochemical processes, particularly the electrochemical potentials for charge/discharge reactions. During a single charging and discharging cycle, misfit strains and stress cause open circuit potential hysteresis, an energy loss during electrochemical cycling. [103]

In this aspect, our team has investigated the rate-dependent mechanical deformations in Li-ion and Na-ion batteries by employing operando digital image correlation and mathematical models. To compare the behavior of Li vs. Na intercalation at faster rates, electrochemical performance and strain generation were also measured in NaFePO<sub>4</sub> and LiFePO<sub>4</sub> cathodes (Figure 4). Both studies employed the

electrode (iron phosphate) as a reference material prepared by the electrochemical displacement method for better comparison. [68,104] NaFePO<sub>4</sub> cathodes suffer from limited practical capacities at faster rates (Figure 4A). The associated strain generation in the NaFePO<sub>4</sub> indicated the additional strain generation in the electrode at faster rates. At the slower rates (C/25), experimentally measured strains agreed with the predicted strains based on open cell theory for anisotropic porous solid end S-combining rule. [72] A transport-mechanics model demonstrated the steeper concentration profile of Na in the electrode particles and associated mismatch strains at faster rates. The practical capacities in LiFePO<sub>4</sub> decreased modestly at faster rates than analogous NaFePO<sub>4</sub> cathodes (Figure 4b). [71] On the other hand, more significant strain evolution per charge/discharge capacity was observed in LiFePO<sub>4</sub> cathodes at faster rates. The electrode was cycled via uninterrupted and pulsed current measurements while monitoring strains in the electrode (Figure 4C). Interestingly, the electrode undergoes more significant mechanical deformations in uninterrupted cycling compared to the pulsed current cycling with periodic open circuit relaxations at the same rate. This district difference in the LiFePO<sub>4</sub> was associated with the peculiar phase transformation behavior of the electrode at faster rates.

There have been several suggestions to mitigate the mechanical deformations in the electrodes at faster rates, including surface modification [105–107] and particle size optimization. [108] Reducing the particle size helps shorten the diffusion pathways in the electrode particles, but the cost of a larger surface area with electrolyte increases manufacturing costs. Various surface coatings have been reported to improve the rate capability of the electrodes, but the underlying physics behind the surface coatings was barely understood. We investigated the role of Au coating on the mechanical stability of LiMn<sub>2</sub>O<sub>4</sub> cathodes at faster rates. Strain measurements indicate smaller deformations in the electrode with Au coating than in uncoated ones. The better rate capability was attributed to the more spatially uniform lithium distribution in the LMO particles with surface coating. [73]

# 3.4. Perspective on Chemo-Mechanical Deformations in Multivalent Batteries

Multivalent-ion batteries are based on shuttling multivalent metal ions such as magnesium, calcium, aluminum, and zinc between electrodes. These battery systems promise a sustainable future for grid storage due to their abundance in the Earth's crust. However, unlike alkali metal ions, the charge carriers are divalent magnesium, calcium, zinc, or trivalent aluminum. [109,110] Storing multivalent ions in electrodes and transporting them between electrodes through electrolyte media is more challenging than the monovalent ion system. These challenges include designing new electrolytes [111–115], preventing dendrite formations on metal anodes [116–119], and exploring cathode structures that can store these ions reversibly. [120–123] Among the multivalent ion batteries, Zinc-based batteries have a long history, with the invention of the Zn-Cu battery in the early 1800s. [124] Zinc-based primary batteries have been developed in the past century, such as Zn-air batteries, alkaline Zn-Mn batteries, and Zn-AgO batteries. These primary batteries account for almost 30% of the commercialized batteries in the world's battery market [125,126]. However, the lack of fundamental understanding of reaction-transport mechanisms limits the design of suitable cathodes and electrolyte chemistries for rechargeable multivalent ion batteries.

On the anode side, the formation of dendrites is the main challenge to improve the cycle life of rechargeable multivalent-ion batteries. [116–119] We foresee that operando DIC and curvature measurements can provide new insights into the dendrite formation mechanisms. Similar to Li metal battery studies as listed above, DIC operando tools can be utilized to probe spatial deformations on metal anodes during the plating/stripping of multivalent ions. Furthermore, operando curvature measurement can provide vital information about nucleation and growth mechanisms for multivalent ion deposition and the onset of elastic/plastic deformations during the dendrite formation.

The electrochemical performance of the cathode materials is still a limiting factor for developing rechargeable multivalent-ion batteries. Instability studies in multivalent cathodes must also consider the impact of electrolyte (organic vs. aqueous) on the charge storage mechanisms and performance decay. For example, even though Yamamoto et al. developed rechargeable Zn-ion batteries by utilizing aqueous electrolytes and MnO<sub>2</sub> cathode in the 1980s, the unknown reaction mechanisms have been a limiting factor for the further developments in aqueous Zn-ion batteries [127–129]. There has been a growing interest in recent years to seek suitable cathode structures for multivalent-ion batteries such as MnO<sub>2</sub> polymorphs [128,130–146], vanadium-based materials [147–154], Mo<sub>6</sub>S<sub>8</sub> [155], Prussian blue analogs [148,156–161] and organic-based cathodes [162]. However, electrochemical performance rechargeable of multivalent-ion batteries suffers from short cycle life

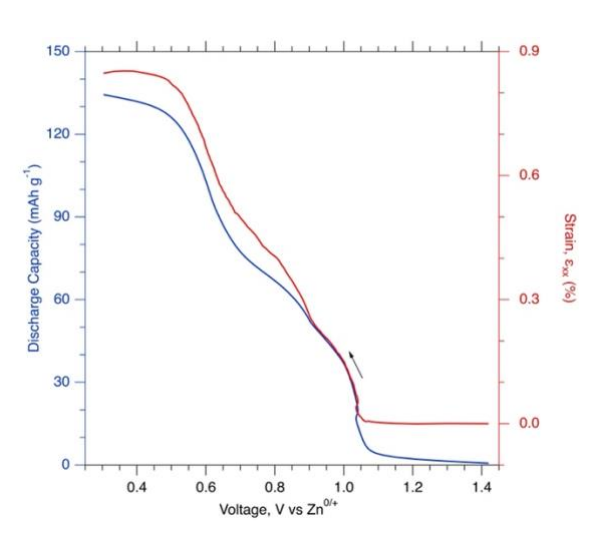


Figure 5: Preliminary studies on mechanics of multivalent ion cathodes. Voltage evolution and strain generation in  $V_2O_5$  during discharge at C/20 rate in an aqueous electrolyte in Zn-ion batteries.

and rapid capacity fade because of chemo-mechanical deformations in cathode materials. The (electrochemical reactions at the cathode/electrolyte interface and charge storage mechanisms in the cathode structure are still significantly debated. Furthermore, there is not much known about mechanical deformations in these cathodes during multivalent ion storage. Understanding multivalent-ion transport and its coupling with interfacial reactivity in cathodes is crucial to achieving reliable long-term performance of aqueous ZIB. In this aspect, we foresee that operando DIC and curvature measurements can be utilized to investigate the charge storage mechanisms, structural instabilities in various states of (dis)-charge, and competition between proton and multivalent ion intercalation into host cathode structure. Our group recently began investigating mechanical deformations in aqueous Zn-ion battery cathodes using these operando tools. Figure 5 demonstrates our preliminary study on strain generation in the  $V_2O_5$  cathode during discharge in aqueous electrolytes for Zn-ion batteries. DIC measurement provided strain generation in the cathode during cycling. Furthermore, the strain evolution shows a strong dependence on the voltage, indicating its high sensitivity to the nano-scale structural changes in the electrode. By using DIC and curvature measurements and carefully designing experimental conditions (e.g., electrode, type of salt and solvent in electrolytes, and cycle conditions), we aim to elucidate the charge storage mechanisms in cathode materials for multivalent ion batteries.

#### 4. CONCLUSION

Operando digital image correlation (DIC) and curvature measurement techniques were used to probe the battery materials' electro-chemical strain and stress generations in alkali metal-ion batteries, all-solidstate batteries, Li-O<sub>2</sub> batteries, and multivalent-ion batteries. In alkali metal-ion batteries, DIC provided information about how different alkali metal ions impact the deformations in graphite, transition metal oxide, olivine-type electrodes, and Prussian blue analogs. Strain analysis indicated that strain rates, rather than nominal strains, are responsible for the amorphization in crystalline electrodes, with the support of in situ X-ray diffraction and electron microscopy studies. Characteristic evolution of micro-scale strain measurement mimics the nano-scale deformations in the electrode structure. Synchronization of stress and strain measurements allows differentiating driving forces dictating surface pressure build-up and structural distortion in the electrodes. Combining X-ray photoelectron spectroscopy with DIC indicated governing mechanisms behind the capacity fade in manganese-based Prussian blue analogs. In all-solidstate batteries, the utilization of operando DIC provides spatial and temporal resolution of deformations in the vicinity of solid electrolyte – Li metal interfaces. The results also indicated the correlation between mechanical deformations and overpotential generation during Li plating in solid electrolytes. Curvature measurements during the discharge of Li-O<sub>2</sub> batteries indicate the interference of the non-faradaic reactions on the electro-chemical reactions. Our preliminary studies on aqueous Zn-ion batteries demonstrate promising features of operando DIC measurements to probe potential-dependent deformations in multivalent battery cathodes. Overall, utilizing DIC and curvature measurements provided novel information about the governing forces behind the chemo-mechanical instabilities of battery materials. We foresee that the unique capability of these mechanical techniques can be utilized to unravel charge storage mechanisms in amorphous electrodes, interfacial instabilities on the electrodeelectrolyte interface, and reaction dynamics in electrocatalytic systems.

# **ACKNOWLEDGEMENT**

Dr. Özgür Çapraz is thankful for the financial support from the U.S. Department of Energy, Office of Science, Basic Energy Sciences (Award number DE-SC0021251) on the alkali-metal ion battery research, National Science Foundation Faculty Early Career Development (CAREER) Program (Award number 2142726) on the instabilities in transmission metal oxide cathodes for Na-ion battery research, Binational Science Foundation (award number 2018327) on the Li-O<sub>2</sub> battery research and NASA (award number 80NSSC19M0058) on the solid-state battery research.

# **AUTHOR CONTRIBUTIONS**

The manuscript was written through the contributions of all authors. All authors have approved the final version of the manuscript. M. W. and B. M. contributed equally, and they can write their name as a first author, as they wish. M. W. and B. M. performed the preliminary experiments on Figure 2D and Figure 5, respectively. The authors declare that they have no competing interests.

# **CONFLICT OF INTEREST**

The authors declare that there is no conflict of interest.

#### **REFERENCES**

- 1. J. B. Goodenough and K.-S. Park, Journal of the American Chemical Society **135**, 1167 (2013).
- 2. P. K. Nayak, L. Yang, W. Brehm, and P. Adelhelm, Angew. Chem. Int. Ed. **57**, 102 (2017).
- 3. Y. Huang, Y. Zheng, X. Li, F. Adams, W. Luo, Y. Huang, and L. Hu, ACS Energy Lett. **3**, 1604 (2018).
- 4. J. Am. Soc. Nav. Eng. 53, 904 (1941).
- 5. K. Kubota, M. Dahbi, T. Hosaka, S. Kumakura, and S. Komaba, Chem Rec 18, 459 (2018).
- 6. K. Kubota, S. Kumakura, Y. Yoda, K. Kuroki, and S. Komaba, Adv Energy Mater **8**, (2018).
- 7. Y.-K. Sun, Acs Energy Lett 5, 3221 (2020).
- 8. A. Banerjee, X. Wang, C. Fang, E. A. Wu, and Y. S. Meng, Chem Rev **120**, 6878 (2020).
- 9. L. Porz, T. Swamy, B. W. Sheldon, D. Rettenwander, T. Frömling, H. L. Thaman, S. Berendts, R. Uecker, W. C. Carter, and Y.-M. Chiang, Advanced Energy Materials **414**, 1701003 (2017).
- 10. M. Aashutosh and P. P. Mukherjee, J. Electrochem Soc. 167, 082510 (2020).
- 11. C. Monroe and J. Newman, J. Electrochem. Soc. **152**, A396 (2005).
- 12. D. Aurbach, B. D. McCloskey, L. F. Nazar, and P. G. Bruce, Nat. Energy 1, 16128 (2016).
- 13. Z. Lyu, Y. Zhou, W. Dai, X. Cui, M. Lai, L. Wang, F. Huo, W. Huang, Z. Hu, and W. Chen, Chem. Soc. Rev. **46**, 6046 (2017).
- 14. D. Sharon, D. Hirsberg, M. Salama, M. Afri, A. A. Frimer, M. Noked, W. Kwak, Y.-K. Sun, and D. Aurbach, ACS Appl. Mater. Interfaces **8**, 5300 (2016).
- 15. B. D. Adams, C. Radtke, R. Black, M. L. Trudeau, K. Zaghib, and L. F. Nazar, Energy Environ. Sci. 6, 1772 (2013).

- 16. Z. Lyu, L. Yang, Y. Luan, X. R. Wang, L. Wang, Z. Hu, J. Lu, S. Xiao, F. Zhang, X. Wang, F. Huo, W. Huang, Z. Hu, and W. Chen, Nano Energy **36**, 68 (2017).
- 17. Z. Peng, S. A. Freunberger, Y. Chen, and P. G. Bruce, Science 337, 1223985 (2012).
- 18. M. M. Thotiyl, S. A. Freunberger, Z. Peng, Y. Chen, Z. Liu, and P. G. Bruce, Nature Materials 12, 1050 (2013).
- 19. Y. Chen, S. A. Freunberger, Z. Peng, O. Fontaine, and P. G. Bruce, Nat Chem 5, 489 (2013).
- 20. Ö. Ö. Çapraz, K. R. Hebert, and P. Shrotriya, J Electrochem Soc 160, D501 (2013).
- 21. J. W. Shin, G. R. Stafford, and K. R. Hebert, Corros Sci 98, 366 (2015).
- 22. Ö. Ö. Çapraz, S. Ide, P. Shrotriya, and K. R. Hebert, Acta Mater 115, 434 (2016).
- 23. G. R. Stafford, O. E. Kongstein, and G. M. Haarberg, J. Electrochem. Soc. 153, C207 (2006).
- 24. M. Fayette, U. Bertocci, and G. R. Stafford, J Electrochem Soc 163, D146 (2016).
- 25. O. E. Kongstein, U. Bertocci, and G. R. Stafford, J. Electrochem. Soc. 152, C116 (2005).
- 26. E. Chason, A. Engwall, F. Pei, M. Lafouresse, U. Bertocci, G. Stafford, J. A. Murphy, C. Lenihan, and D. N. Buckley, Journal of the Electrochemical Society **160**, D3285 (2013).
- 27. A. Mukhopadhyay and B. W. Sheldon, Prog Mater Sci 63, 58 (2014).
- 28. J. H. Cho, X. Xiao, K. Guo, Y. Liu, H. Gao, and B. W. Sheldon, Energy Storage Mater **24**, 281 (2020).
- 29. Y. Song, B. Bhargava, D. M. Stewart, A. A. Talin, G. W. Rubloff, and P. Albertus, Joule 7, 652 (2023).
- 30. Y. Zhang, Y. Luo, C. Fincher, S. McProuty, G. Swenson, S. Banerjee, and M. Pharr, Energy Storage Mater 16, 491 (2019).
- 31. S. Rakshit, A. S. Pakhare, O. Ruiz, M. R. Khoshi, E. Detsi, H. He, V. A. Sethuraman, and S. P. V. Nadimpalli, J. Electrochem. Soc. **168**, 010504 (2021).
- 32. T. T. H. Hoang, Y. Cohen, and A. A. Gewirth, Analytical Chemistry 86, 11290 (2014).

- 33. Y. Ha, J. L. Oberst, Z. Zeng, T. T. H. Hoang, Y. Cohen, D. J. Wetzel, R. G. Nuzzo, J. Greeley, and A. A. Gewirth, Electrochimica Acta **260**, 400 (2018).
- 34. Y. Ha, Z. Zeng, Y. Cohen, J. Greeley, and A. A. Gewirth, J Phys Chem C **120**, 8674 (2016).
- 35. V. A. Sethuraman, D. Vairavapandian, M. C. Lafouresse, T. A. Maark, N. Karan, S. Sun, U. Bertocci, A. A. Peterson, G. R. Stafford, and P. R. Guduru, J. Phys. Chem. C 119, 19042 (2015).
- 36. Q. Deng and J. Weissmüller, Langmuir **30**, 10522 (2014).
- 37. R. N. Viswanath, D. Kramer, and J. Weissmüller, Electrochimica Acta **53**, 2757 (2008).
- 38. D. Kramer and J. Weissmüller, Surface Science 601, 3042 (2007).
- 39. Q. Yang and J. D. Nicholas, J Electrochem Soc 161, F3025 (2014).
- 40. Nicholas, JD. In situ Wafer Curvature Relaxation Measurements to Determine Surface Exchange Coefficients and Thermo-Chemically Induced Stresses. In Bishop, S., Marriochelli, D., Perry, N. and Sheldon, B., eds. Electro-Chemo-Mechanics of Solids, pp. 103-106 (Springer, New York, 2017). ISBN: 978-3-319-51405-5 (Print) 41. G. G. Stoney, Proceedings of the Royal Society A: Mathematical, Physical and Engineering Sciences 82, 172 (1909).
- 42. C. A. Klein, Journal of Applied Physics **88**, 5487 (2000).
- 43. G. C. A. M. Janssen, M. M. Abdalla, F. van Keulen, B. R. Pujada, and B. van Venrooy, Thin Solid Films **517**, 1858 (2009).
- 44. K. Ueno, J. Electrochem. Soc. 146, 1496 (1999).
- 45. W. Haiss, Reports on Progress in Physics 64, 591 (2001).
- 46. M. Seo and Y. Serizawa, J. Electrochem. Soc. **150**, E472 (2003).
- 47. J. L. Langer, J. Economy, and D. G. Cahill, Macromolecules 45, 3205 (2012).
- 48. X. Zhang and D. G. Cahill, Langmuir **22**, 9062 (2006).
- 49. H. Tavassol, M. K. Y. Chan, M. G. Catarello, J. Greeley, D. G. Cahill, and A. A. Gewirth, J Electrochem Soc **160**, A888 (2013).

- 50. J. A. Floro and E. Chason, Phys. Rev. Lett. 88, 156103 (2002).
- 51. H. Dykes, Rosy, D. Sharon, M. Noked, and Ö. Çapraz, J Electrochem Soc **168**, 110551 (2021).
- 52. M. Sutton, C. Mingqi, W. Peters, Y. Chao, and S. McNeill, Image Vis. Comput. 4, 143 (1986).
- 53. Y. Qi and S. J. Harris, Journal of the Electrochemical Society 157, A741 (2010).
- 54. D. S. Eastwood, V. Yufit, J. Gelb, A. Gu, R. S. Bradley, S. J. Harris, D. J. L. Brett, N. P. Brandon, P. D. Lee, P. J. Withers, and P. R. Shearing, Advanced Energy Materials 4, 1300506 (2013).
- 55. E. M. C. Jones, M. N. Silberstein, S. R. White, and N. R. Sottos, Exp Mech **54**, 971 (2014).
- 56. H. Tavassol, E. M. C. Jones, N. R. Sottos, and A. A. Gewirth, Nat Mater 15, 1182 (2016).
- 57. E. Jones, O. Capraz, and N. Sottos, J. Eletrochem. Soc. 163, A1965-A1974 (2016).
- 58. B. Koohbor, L. Sang, Ö. Ö. Çapraz, A. A. Gewirth, and N. R. Sottos, J Electrochem Soc **168**, 010516 (2021).
- 59. B. Koohbor, L. Sang, Ö. Ö. Çapraz, A. A. Gewirth, R. G. Nuzzo, S. R. White, and N. R. Sottos, in (Springer International Publishing, 2018), pp. 1–3.
- 60. W. Zhang, Y. Liu, and Z. Guo, Sci. Adv. 5, eaav7412 (2019).
- 61. K. Xiang, W. Xing, D. B. Ravnsbæk, L. Hong, M. Tang, Z. Li, K. M. Wiaderek, O. J. Borkiewicz, K. W. Chapman, P. J. Chupas, and Y.-M. Chiang, Nano Lett. 17, 1696 (2017).
- 62. Z. Li, B. Ozdogru, B. Bal, M. Bowden, A. Choi, Y. Zhang, H. Wang, V. Murugesan, V. G. Pol, and Ö. Ö. Çapraz, Adv. Energy Mater. 13, (2023).
- 63. K. Dokko, M. Mohamedi, Y. Fujita, T. Itoh, M. Nishizawa, M. Umeda, and I. Uchida, J. Electrochem. Soc. **148**, A422 (2001).
- 64. D. Wang, X. Wu, Z. Wang, and L. Chen, Journal of Power Sources **140**, 125 (2005).
- 65. Z. Zhang, Z. Chen, G. Wang, H. Ren, M. Pan, L. Xiao, K. Wu, L. Zhao, J. Yang, Q. Wu, J. Shu, D. Wang, H. Zhang, N. Huo, and J. Li, Physical Chemistry Chemical Physics 18, 6893 (2016).

- 66. D. A. Gribble, Z. Li, B. Ozdogru, E. McCulfor, Ö. Ö. Çapraz, and V. G. Pol, Adv Energy Mater **12**, 2103439 (2022).
- 67. B. Özdogru, B. Koohbor, and Ö. Ö. Çapraz, Electrochem Sci Adv, **2**, 4, e2100106 (2021).
- 68. B. Özdogru, H. Dykes, S. Padwal, S. Harimkar, and Ö. Ö. Çapraz, Electrochimica Acta **353**, 136594 (2020).
- 69. K. L. Bassett, Ö. Ö. Çapraz, B. Özdogru, A. A. Gewirth, and N. R. Sottos, Journal of the Electrochemical Society **166**, A2707 (2019).
- 70. Ö. Ö. Çapraz, S. Rajput, S. White, and N. R. Sottos, Experimental Mechanics 15, 1182 (2018).
- 71. B. Ozdogru; M. Vijayakumar, and Ö. Ö. Çapraz, Journal of Materials Research, **37**, 3237–3248 (2022)
- 72. B. Özdogru, H. Dykes, D. Gregory, D. Saurel, V. Murugesan, M. Casas-Cabanas, and Ö. Ö. Çapraz, J Power Sources **507**, 230297 (2021).
- 73. Ö. Ö. Çapraz, S. Rajput, K. L. Bassett, A. A. Gewirth, S. R. White, and N. R. Sottos, Journal of the Electrochemical Society **166**, A2357 (2019).
- 74. B. Özdogru, Y. Cha, B. Gwalani, V. Murugesan, M.-K. Song, and O. O. Çapraz, Nano Lett **21**, 7579 (2021).
- 75. S. Wang, F. Chen, T. Zhu, X. He, J. Liao, L. Zhang, X. Ding, Q. Hu, and C. Chen, ACS Appl. Mater. Interfaces **12**, 44671 (2020).
- 76. Ö. Ö. Çapraz, K. L. Bassett, A. A. Gewirth, and N. R. Sottos, Advanced Energy Materials 1601778 (2016).
- 77. N. Ohmer, B. Fenk, D. Samuelis, C.-C. Chen, M. Weigand, E. Goering, J. Maier, and G. S. uuml tz, Nature Communications **6**, 1 (2015).
- 78. K. Xu, Chem. Rev. **114**, 11503 (2014).
- 79. K. Xu, ChemInform **35**, no (2004).
- 80. S. Komaba, W. Murata, T. Ishikawa, N. Yabuuchi, T. Ozeki, T. Nakayama, A. Ogata, K. Gotoh, and K. Fujiwara, Adv. Funct. Mater. **21**, 3859 (2011).
- 81. A. Ponrouch, E. Marchante, M. Courty, J.-M. Tarascon, and M. R. Palacín, Energy Environ. Sci. 5, 8572 (2012).

- 82. R. Mogensen, J. Maibach, W. R. Brant, D. Brandell, and R. Younesi, Electrochimica Acta **245**, 696 (2017).
- 83. J. Song, B. Xiao, Y. Lin, K. Xu, and X. Li, Adv. Energy Mater. 8, 1703082 (2018).
- 84. K. Lei, F. Li, C. Mu, J. Wang, Q. Zhao, C. Chen, and J. Chen, Energy Environ. Sci. **10**, 552 (2017).
- 85. A. J. Naylor, M. Carboni, M. Valvo, and R. Younesi, ACS Appl. Mater. Interfaces 11, 45636 (2019).
- 86. D. A. Wynn, M. M. Roth, and B. D. Pollard, Talanta 31, 1036 (1984).
- 87. M. Moshkovich, Y. Gofer, and D. Aurbach, J. Electrochem. Soc. 148, E155 (2001).
- 88. S. Chong, Y. Wu, S. Guo, Y. Liu, and G. Cao, Energy Storage Mater 22, 120 (2019).
- 89. S. Chong, J. Yang, L. Sun, S. Guo, Y. Liu, and H. K. Liu, Acs Nano 14, 9807 (2020).
- 90. L. Li, Z. Hu, Y. Lu, C. Wang, Q. Zhang, S. Zhao, J. Peng, K. Zhang, S. Chou, and J. Chen, Angew. Chem. Int. Ed. **60**, 13050 (2021).
- 91. P. Wang, W. Qu, W. Song, H. Chen, R. Chen, and D. Fang, Adv Funct Mater **29**, 1900950 (2019).
- 92. J. A. Lewis, J. Tippens, F. J. Q. Cortes, and M. T. McDowell, Trends Chem. 1, 845 (2019).
- 93. M. G. Boebinger, J. A. Lewis, S. E. Sandoval, and M. T. McDowell, ACS Energy Lett. 5, 335 (2020).
- 94. M. T. McDowell, MRS Bull. 45, 889 (2020).
- 95. M. T. McDowell, F. J. Q. Cortes, A. C. Thenuwara, and J. A. Lewis, Chem. Mater. **32**, 8755 (2020).
- 96. B. Ozdogru, S. Padwal, B. Bal, S. Harimkar, B. Koohbor, and Ö. Ö. Çapraz, ACS Applied Energy Materials, 5, 3, 2655–2662 (2022).
- 97. E. Chason, B. W. Sheldon, L. B. Freund, J. A. Floro, and S. J. Hearne, Physical Review Letters 88, 689 (2002).
- 98. E. Chason, Thin Solid Films **526**, 1 (2012).
- 99. J. W. Shin and E. Chason, Physical Review Letters 103, 19 (2009).

- 100. E. Chason, A. M. Engwall, C. M. Miller, C. H. Chen, A. Bhandari, S. K. Soni, S. J. Hearne, L. B. Freund, and B. W. Sheldon, SMM **97**, 33 (2015).
- 101. K. Zhao, M. Pharr, J. J. Vlassak, and Z. Suo, J Appl Phys 108, 073517 (2010).
- 102. W. H. Woodford, W. C. Carter, and Y. M. Chiang, J. Electrochem. Soc. **161**, F3005 (2014).
- 103. B. W. Sheldon, S. K. Soni, X. Xiao, and Y. Qi, Electrochem Solid-State Lett 15, A9 (2012).
- 104. C. Heubner, S. Heiden, B. Matthey, M. Schneider, and A. Michaelis, Electrochimica Acta **216**, 412 (2016).
- 105. D. Tang, R. Yi, M. L. Gordin, M. Melnyk, F. Dai, S. Chen, J. Song, and D. Wang, Journal of Materials Chemistry A 2, 10375 (2014).
- 106. J. Li, Y. Zhu, L. Wang, and C. Cao, Acs Appl Mater Inter 6, 18742 (2014).
- 107. C. Zhang, X. Liu, Q. Su, J. Wu, T. Huang, and A. Yu, ACS Sustainable Chemistry & Engineering 5, 640 (2017).
- 108. Y.-T. Cheng and M. W. Verbrugge, J Appl Phys **104**, 083521 (2008).
- 109. Y. Liang, H. Dong, D. Aurbach, and Y. Yao, Nat. Energy 5, 646 (2020).
- 110. S. Zhang, T. Long, H. Zhang, Q. Zhao, F. Zhang, X. Wu, and X. Zeng, ChemSusChem **15**, e202200999 (2022).
- 111. J. Zhang, X. Yao, R. K. Misra, Q. Cai, and Y. Zhao, J Mater Sci Technol 44, 237 (2020).
- 112. K. Huang, Z.; K. Yao; K. Sun; K. Chen; J. Hu; D. Yin, and; C. Li, J. Power Sources **482**, 228904 (2021).
- 113. S.-B. Son, T. Gao, S. P. Harvey, K. X. Steirer, A. Stokes, A. Norman, C. Wang, A. Cresce, K. Xu, and C. Ban, Nature Chemistry 10, 1 (2018).
- 114. S. C. Bevilacqua, K. H. Pham, and K. A. See, Inorganic Chemistry 58, 10472 (2019).
- 115. K. A. See, K. W. Chapman, L. Zhu, K. M. Wiaderek, O. J. Borkiewicz, C. J. Barile, P. J. Chupas, and A. A. Gewirth, Journal of the American Chemical Society **138**, 328 (2016).
- 116. D. Gregory, C. Britten, B. Bal, B. S. Abbott, B. Özdogru, K. B. Walters, and Ö. Ö. Çapraz, ChemElectroChem, **9**, 4, e202101121 (2021).

- 117. I. D. Hosein, ACS Energy Lett. 6, 1560 (2021).
- 118. J. H. Kwak, Y. Jeoun, S. H. Oh, S. Yu, J.-H. Lim, Y.-E. Sung, S.-H. Yu, and H.-D. Lim, ACS Energy Lett. **7**, 162 (2022).
- 119. Y. Long, H. Li, M. Ye, Z. Chen, Z. Wang, Y. Tao, Z. Weng, S.-Z. Qiao, and Q.-H. Yang, Energy Storage Mater. **34**, 194 (2021).
- 120. Z. Ma, D. R. MacFarlane, and M. Kar, Batteries & Supercaps 19, 291 (2019).
- 121. M. Mao, T. Gao, S. Hou, and C. Wang, Chem Soc Rev 47, 8804 (2018).
- 122. Y. Yang, J. Zhou, L. Wang, Z. Jiao, M. Xiao, Q. Huang, M. Liu, Q. Shao, X. Sun, and J. Zhang, Nano Energy **99**, 107424 (2022).
- 123. Z. Zhang, X. Zhang, X. Zhao, S. Yao, A. Chen, and Z. Zhou, ACS Omega 4, 7822 (2019).
- 124. A. Volta, Philosophical Transactions Royal Soc Lond 90, 403 (1800).
- 125. Y. Shi, Y. Chen, L. Shi, K. Wang, B. Wang, L. Li, Y. Ma, Y. Li, Z. Sun, W. Ali, and S. Ding, Small **16**, 2000730 (2020).
- 126. H. Li, L. Ma, C. Han, Z. Wang, Z. Liu, Z. Tang, and C. Zhi, Nano Energy **62**, 550 (2019).
- 127. T. Shoji and T. Yamamoto, J Electroanal Chem 362, 153 (1993).
- 128. T. Yamamoto and T. Shoji, Inorg Chim Acta 117, L27 (1986).
- 129. T. Shoji, M. Hishinuma, and T. Yamamoto, J Appl Electrochem 18, 521 (1988).
- 130. J. Shin, J. K. Seo, R. Yaylian, A. Huang, and Y. S. Meng, Int Mater Rev **65**, 1 (2019).
- 131. J. McBreen, Electrochim Acta **20**, 221 (1975).
- 132. W. C. Maskell, J. E. A. Shaw, and F. L. Tye, Electrochim Acta 26, 1403 (1981).
- 133. M. A. Dzieciuch, N. Gupta, and H. S. Wroblowa, J Electrochem Soc 135, 2415 (1988).
- 134. Y. Chabre and J. Pannetier, Prog Solid State Ch 23, 1 (1995).
- 135. L. Binder, K. Kordesch, and P. Urdl, J Electrochem Soc 143, 13 (1996).

- 136. S. H. Kim and S. M. Oh, J Power Sources **72**, 150 (1998).
- 137. C.-C. Yang and S.-J. Lin, J Power Sources 112, 174 (2002).
- 138. M. Manickam, P. Singh, T. B. Issa, S. Thurgate, and R. D. Marco, J Power Sources **130**, 254 (2004).
- 139. J. P. Tafur, J. Abad, E. Román, and A. J. F. Romero, Electrochem Commun **60**, 190 (2015).
- 140. B. Lee, H. R. Lee, H. Kim, K. Y. Chung, B. W. Cho, and S. H. Oh, Chem Commun **51**, 9265 (2015).
- 141. N. Zhang, F. Cheng, Y. Liu, Q. Zhao, K. Lei, C. Chen, X. Liu, and J. Chen, J Am Chem Soc **138**, 12894 (2016).
- 142. J. W.; Gallaway, G. G.; Yadav, D. E.; Turney, M.; Nyce, J.; Huang, Y. K.; Chen-Wiegart, G.; Williams, J.; Thieme, J. S.; Okasinski, X.; Wei, and S.; Banarjee, J. Electrochem. Soc. 13, A2935 (2018).
- 143. S.-D. Han, S. Kim, D. Li, V. Petkov, H. D. Yoo, P. J. Phillips, H. Wang, J. J. Kim, K. L. More, B. Key, R. F. Klie, J. Cabana, V. R. Stamenkovic, T. T. Fister, N. M. Markovic, A. K. Burrell, S. Tepavcevic, and J. T. Vaughey, Chem Mater **29**, 4874 (2017).
- 144. W. Sun, F. Wang, S. Hou, C. Yang, X. Fan, Z. Ma, T. Gao, F. Han, R. Hu, M. Zhu, and C. Wang, J Am Chem Soc **139**, 9775 (2017).
- 145. T. Le, N. Sadique, L. M.; Housel, A. S.; Poyraz, E. S.; Takeuchi, K. J.; Takeuchi, A. C.; Marschilok, and P. Liu, ACS Applied Materials & Interfaces 59937 (2021).
- 146. M. H. Alfaruqi, S. Islam, D. Y. Putro, V. Mathew, S. Kim, J. Jo, S. Kim, Y.-K. Sun, K. Kim, and J. Kim, Electrochim Acta **276**, 1 (2018).
- 147. D. Kundu, B. D. Adams, V. Duffort, S. H. Vajargah, and L. F. Nazar, Nat Energy 1, 16119 (2016).
- 148. M. Zhang, R. Liang, T. Or, Y.-P. Deng, A. Yu, and Z. Chen, Small Struct 2, 2000064 (2021).
- 149. J. Ding, Z. Du, L. Gu, B. Li, L. Wang, S. Wang, Y. Gong, and S. Yang, Adv Mater **30**, 1800762 (2018).
- 150. L. Zhang, I. A. Rodríguez-Pérez, H. Jiang, C. Zhang, D. P. Leonard, Q. Guo, W. Wang, S. Han, L. Wang, and X. Ji, Adv Funct Mater **29**, 1902653 (2019).

- 151. M. H. Alfaruqi, V. Mathew, J. Song, S. Kim, S. Islam, D. T. Pham, J. Jo, S. Kim, J. P. Baboo, Z. Xiu, K.-S. Lee, Y.-K. Sun, and J. Kim, Chem Mater **29**, 1684 (2017).
- 152. N. Zhang, M. Jia, Y. Dong, Y. Wang, J. Xu, Y. Liu, L. Jiao, and F. Cheng, Adv Funct Mater **29**, 1807331 (2019).
- 153. Y. Liu, Y. Zou, M. Guo, Z. Hui, and L. Zhao, Chem Eng J 433, 133528 (2022).
- 154. M. Yan, P. He, Y. Chen, S. Wang, Q. Wei, K. Zhao, X. Xu, Q. An, Y. Shuang, Y. Shao, K. T. Mueller, L. Mai, J. Liu, and J. Yang, Adv Mater **30**, 1703725 (2018).
- 155. M. S. Chae, J. W. Heo, S.-C. Lim, and S.-T. Hong, Inorg Chem 55, 3294 (2016).
- 156. Q. Yang, F. Mo, Z. Liu, L. Ma, X. Li, D. Fang, S. Chen, S. Zhang, and C. Zhi, Adv Mater **31**, 1901521 (2019).
- 157. J. Yan, E. H. Ang, Y. Yang, Y. Zhang, M. Ye, W. Du, and C. C. Li, Adv Funct Mater **31**, 2010213 (2021).
- 158. G. Kasiri, R. Trócoli, A. B. Hashemi, and F. L. Mantia, Electrochim Acta 222, 74 (2016).
- 159. G. Ni, B. Han, Q. Li, Z. Ji, B. Huang, and C. Zhou, Chemelectrochem 3, 798 (2016).
- 160. M. S. Chae, J. W. Heo, H. H. Kwak, H. Lee, and S.-T. Hong, Journal of Power Sources **337**, 204 (2017).
- 161. R. Trócoli and F. La Mantia, Chemsuschem 8, 481 (2015).
- 162. E.; Grignon, A. M.; Battaglia, T. B.; Schon, and D. S.; Seferos, IScience, **25**, 5, 104204 (2022).